CDDpress

www.nature.com/cdd

ARTICLE

DCC/netrin-1 regulates cell death in oligodendrocytes after brain injury

Madelen M. Díaz[1], Yanina Tsenkina[1], Dena Arizanovska[1], Patrick Mehlen[2]✉ and Daniel J. Liebl[1]✉

© The Author(s), under exclusive licence to ADMC Associazione Differenziamento e Morte Cellulare 2022

Hallmark pathological features of brain trauma are axonal degeneration and demyelination because myelin-producing oligodendrocytes (OLs) are particularly vulnerable to injury-induced death signals. To reveal mechanisms responsible for this OL loss, we examined a novel class of "death receptors" called dependence receptors (DepRs). DepRs initiate pro-death signals in the absence of their respective ligand(s), yet little is known about their role after injury. Here, we investigated whether the deleted in colorectal cancer (DCC) DepR contributes to OL loss after brain injury. We found that administration of its netrin-1 ligand is sufficient to block OL cell death. We also show that upon acute injury, DCC is upregulated while netrin-1 is downregulated in perilesional tissues. Moreover, after genetically silencing pro-death activity using *DCC*^{D1290N} mutant mice, we observed greater OL survival, greater myelin integrity, and improved motor function. Our findings uncover a novel role for the netrin-1/DCC pathway in regulating OL loss in the traumatically injured brain.

Cell Death & Differentiation (2023) 30:397–406; https://doi.org/10.1038/s41418-022-01091-z

INTRODUCTION

Traumatic brain injury (TBI) is a "silent epidemic" affecting ~69 million people worldwide each year [1]. In 2017, TBIs were responsible for about 2.2% of all deaths within the United States, which translates to over 61,000 casualties [2]. Surviving patients often suffer cognitive and neurological impairments [3, 4], which is also observed in murine models of TBI [5–7]. Such long-term deficits are a result of secondary damage persisting for several days, months or even years, exacerbating cell death, axonal destruction, and demyelination [8–10]. Notably, myelin-producing oligodendrocytes (OLs) are exceptionally vulnerable to injury, where significant cell loss has been observed as soon as 4–6 h post injury (hpi) in neurotrauma patients [11] and mice following controlled cortical impact (CCI) injury [12]. This OL loss further contributes to axonal damage, demyelination, and other white matter pathologies in TBI [13–17]. Despite extensive research in cell death signaling, few studies have examined the underlying mechanism of OL cell loss after injury.

Traditional cell death receptors, such as Fas and TNF-R1, promote apoptosis upon ligand activation [18–25]. However, clinical trials targeting traditional death receptors have been underwhelming [26–33], likely indicating that there are additional pro-apoptotic signaling mechanisms. Another family of receptors called dependence receptors (DepRs) have been strongly implicated to be pro-apoptotic in cancer biology [34–39], neurodegenerative diseases [40–43], spinal cord injury [44, 45], and brain injury [12, 46–48]. In contrast to the more classical death receptors, DepRs depend on their respective ligand binding activity to either actively promote apoptotic signaling (i.e., in the absence of ligand), or to inhibit this apoptotic signaling (i.e., in the presence of ligand) [49]. For instance, we have shown that the ephrin-B3 ligand is required to prevent EphB3-mediated cell loss of cortical neurons [47], endothelial cells [48], and mature OLs [12] after brain injury. Given the increasing evidence of DepR-mediated apoptosis, we examined whether other classes of DepRs also contribute to OL cell death in the traumatically injured brain.

Deleted in Colorectal Cancer (DCC) is a transmembrane receptor that exhibits dual signaling depending on the availability of its ligand, netrin-1 [50–52]. Netrin-1/DCC has been extensively implicated in promoting positive signals such as cell survival, proliferation, and migration [51, 53–56]. However, DCC can trigger cell death when netrin-1 is disengaged [34, 51, 57–60], thereby acting as a DepR. Caspase recruitment and proteolytic cleavage of the DCC receptor occurs in the conserved aspartic acid residue at 1290 [34, 61]. By mutating this single amino acid from an aspartic acid to an asparagine (*DCC*^{D1290N}), this proteolytic cleavage is genetically blocked, therefore exclusively ablating DCC-induced apoptosis [34, 62]. Previous studies have shown that mice harboring this point mutation are susceptible to different types of cancers [62–64], highlighting DCC's role in regulating cell survival and death.

Here, we show that DCC is highly enriched in OLs, and that netrin-1 administration can promote OL survival after inducing cell death. In particular, *DCC*^{D1290N} mutant mice exhibited attenuated OL cell loss in the injured penumbra that resulted in improved myelin integrity and motor coordination after CCI injury.

[1]The Miami Project to Cure Paralysis, Department of Neurosurgery, University of Miami Miller School of Medicine, Miami, FL, USA. [2]Apoptosis, Cancer and Development Laboratory – Equipe labellisée 'La Ligue', LabEx DEVweCAN, Centre de Recherche en Cancérologie de Lyon, INSERM U1052-CNRS UMR5286, Centre Léon Bérard, Université de Lyon, Université de Lyon1, Lyon, France. ✉email: patrick.mehlen@lyon.unicancer.fr; dliebl@miami.edu

Edited by M Piacentini

Received: 8 December 2021 Revised: 7 November 2022 Accepted: 11 November 2022
Published online: 1 December 2022

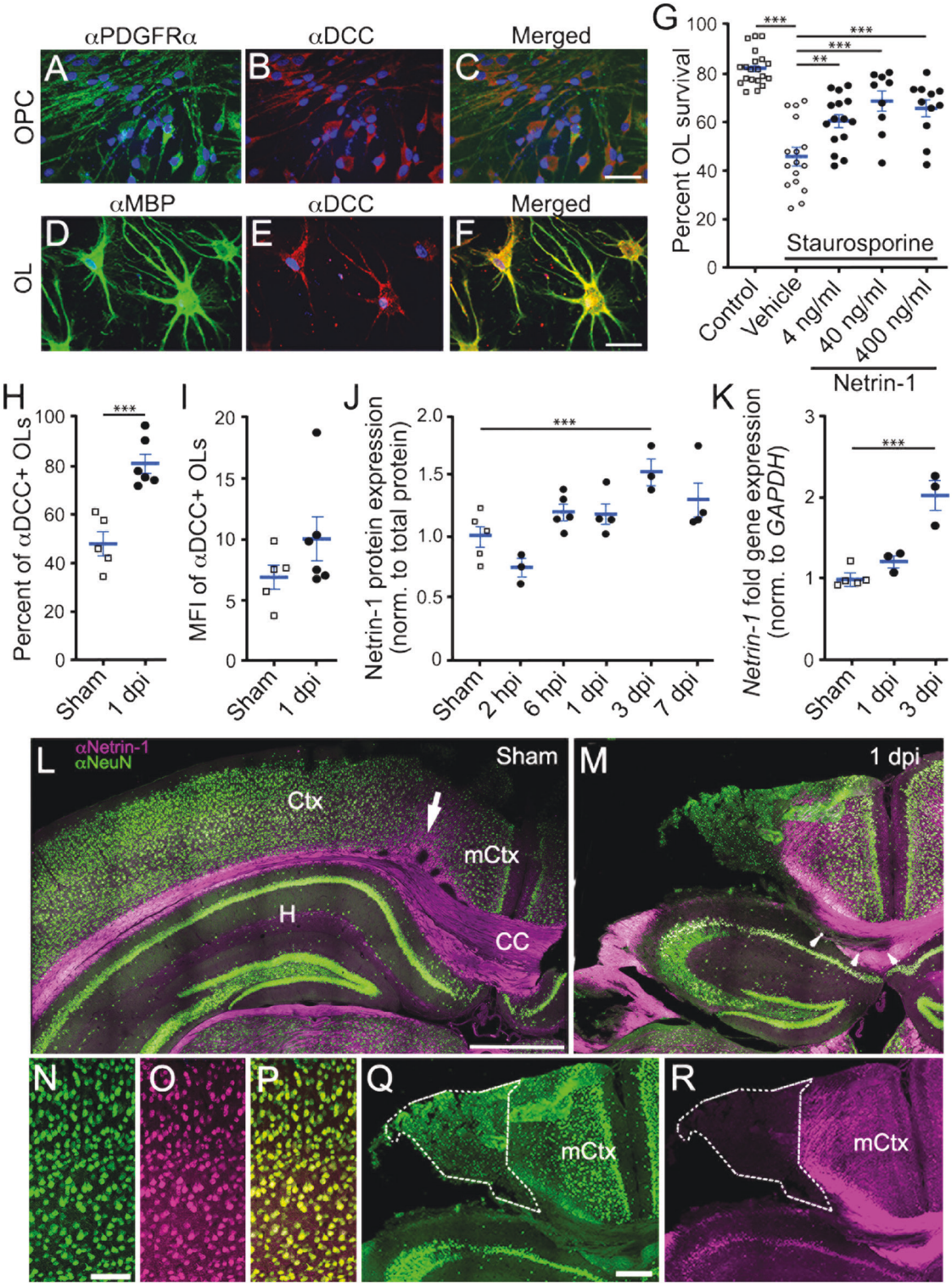

RESULTS

Netrin-1/DCC receptor mediates stress-induced oligodendrocyte (OL) cell death in vitro

To confirm whether DCC receptors function as DepRs in OLs, we initially examined DCC receptor expression in vitro. Oligodendrocyte progenitor cells (OPCs) were derived from the adult mouse CNS and subsequently differentiated into mature OLs (Fig. 1) as previously described [45]. OPCs were identified as bipolar cells expressing both A2B5 (not shown) and platelet-derived growth factor receptor (PDGFRα; Fig. 1A), while OLs expressed the O1, O4, GalC antigens (not shown), and myelin basic protein (MBP; Fig. 1D). Consistent with previous findings [56], Fig. 1A–F shows that DCC receptors are expressed in cultured OPCs and OLs.

To provide evidence that DCC has DepR functions in OLs, we examined whether application of netrin-1 could block DCC-mediated cell death in primary OLs. Cell stress was induced using staurosporine as previously described [45, 47]. Staurosporine induces cell death by involving caspase-dependent mechanisms, a

Fig. 1 DCC receptors are expressed by oligodendrocytes (OLs) and are dependent on netrin-1 for survival. A–F Representative images showing DCC (**B**, **E**) is expressed in both PDGFRα-labeled oligodendrocyte progenitor cells (OPCs) (**A**) and myelin basic protein (MBP)-positive mature OLs (**D**) in vitro. Blue channel indicates DAPI signal. Scale bar represents 10 µm. **G** Netrin-1 dose-dependent (4, 40, 400 ng/mL) administration protects cultured mature OLs from 20 nM Staurosporine-induced cell death ($n = 9$–20). **H**,**I** The percentage of DCC receptors in total OLs (**H**) and mean fluorescent intensity (MFI) per OL (**I**) are increased in FACS cortical O1$^+$ OLs at 1-day post-CCI injury (dpi) ($n = 6$) as compared to sham controls ($n = 5$). **J** Western blot analysis shows increased netrin-1 expression at only 3 dpi ($n = 3$–5). **K** Fold change of *netrin-1* mRNA transcripts from sham, 1 dpi, and 3 dpi WT cortices ($n = 3$–5). **L**–**R** Representative coronal images of αNetrin-1 (magenta) co-labeling with αNeuN + neurons (green) in WT sham (**L**, **N**–**P**) and 1 dpi (**M**, **Q**, **R**) mouse tissues. **L** αNetrin-1 has widespread expression in the cortex, white matter tracts, and subcortical regions. Arrow denotes the apex of the CC, which designates our definition of the medial cortex (mCtx) from other lateral cortical tissues. **M** αNetrin-1 labeling is not detectable in regions of the ventral CC (arrowheads) and perilesional tissues (white outline, **Q**–**R**) at 1 dpi. Scale bars are 500 µm (**L**–**M**), or 50 µm (**N**–**R**). Values represent mean ± SEM. One-way ANOVA with Bonferroni's multiple comparison test or Welsh's unpaired, two-tailed *t*-test. *$p < 0.05$, **$p < 0.01$, ***$p < 0.001$. Ctx: cortex, CC: corpus callosum, H: hippocampus.

necessary activation step for initiating DepR mechanisms [34, 65]. After 48 h of 20 nM staurosporine administration, there was a significant reduction in OL survival (45.6% ± 3.6 survival, $n = 16$) as compared to untreated groups (81.9% ± 1.6 survival, $n = 20$) (Fig. 1G). Administration of netrin-1 significantly blocked OL cell death following staurosporine exposure (~15–23% increase from vehicle administration), although dosing concentrations ranging between 4 and 400 ng/mL netrin-1 showed no significant differences. This suggests that 4 ng/ml of netrin-1 is sufficient to partially block staurosporine-induced OL cell death and supports a role for the pair netrin-1/DCC DepR in regulating OL survival/death following cellular stress.

Netrin-1 and DCC receptor expression is increased in OLs after CCI injury

Evidence for DCC receptor expression in OLs in vivo comes from a single-cell RNA sequencing dataset [66], where *DCC* transcripts were enriched in OLs in the adult mouse CNS glia (Fig. S1A) with little astrocyte or microglia expression. To provide cell-specific protein confirmation, we employed flow cytometry antibody labeling (Fig. S1B–H) to probe for the extracellular domain of DCC in viable cortical microglia, astrocytes, and OLs. We observed a similar expression profile for the protein as the mRNA, where αDCC labeling was most abundant in O1$^+$ OLs (47.7% ± 4.9, $n = 5$) as compared to ACSA-2$^+$ astrocytes (1.0% ± 0.5, $n = 5$) or CD45^{Low}/CD11b$^+$ microglia (5.1% ± 0.5, $n = 5$) within the adult mouse cortex (Fig. S1B).

We next examined whether brain trauma altered DCC receptor expression by employing a well-established CCI model to induce a moderate contusion injury over the parieto-temporal cortex [67] (Figs. 1M and 2B). By probing for αDCC labeling via flow cytometry, we found that DCC receptor expression was significantly increased in viable O1$^+$ OLs at 1 dpi (80.7% ± 4.0, $n = 6$) (Fig. 1H; Fig. S1B). In addition, the average median fluorescent intensity (MFI) per OL cell was increased at 1 dpi as compared to sham control (Fig. 1I).

To further evaluate the status of the DCC dependence receptor function after injury, we probed for the status of the netrin-1 ligand in the injured cortex. Because netrin-1 is a secreted factor [68], we used the ipsilateral cortex of sham and CCI injured WT mice to examine relative netrin-1 protein levels and *netrin-1* mRNA transcripts. In whole ipsilateral cortical tissues, we observed increased netrin-1 levels at 3 dpi, but not between 2 h post-injury (hpi) and 1 dpi (Fig. 1J; Fig. S3), a time point when DCC levels are increased (Fig. 1H, I). This increased netrin-1 levels at 3 dpi is observed in spared tissues. By 7 dpi, Netrin-1 expression returned to pre-injury levels. Similarly, *netrin-1* mRNA transcripts were not significantly different at 1 dpi (1.2 ± 0.07, $n = 3$), but were significantly upregulated at 3 dpi (2.0 ± 0.18, $n = 3$) compared to sham mice (1.0 ± 0.05, $n = 5$) (Fig. 1K). To provide spatial evaluation of netrin-1 expression, we perform αNetrin-1 and αNeuN co-labeling immunohistochemical analysis (Fig. 1L–R). Sham mice (Fig. 1L, N–P) showed Netrin-1 expression was

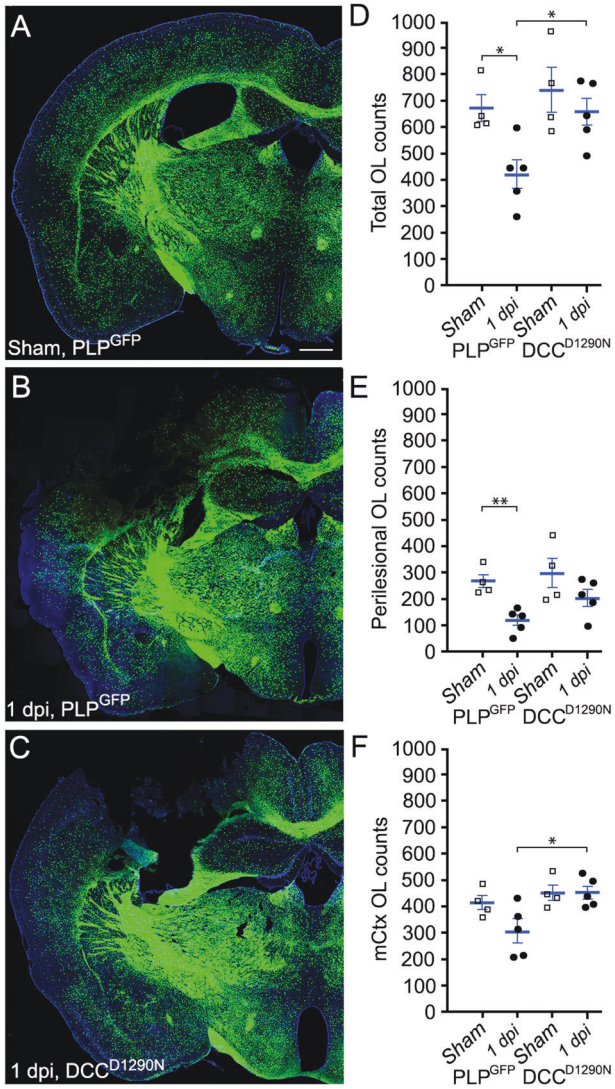

Fig. 2 *DCC^{D1290N}* mice have reduced OL cell death after CCI injury. A–C Representative coronal images of a control sham brain (**A**), and a CCI-injured brain from a *PLP^{GFP}* mice (**B**) and *DCC^{D1290N}*:*PLP^{GFP}* mice (**C**) at 1 dpi. The injury epicenter is noted by the loss of tissue and GFP-fluorescence. Blue channel indicates DAPI signal. Scale bar represents 500 µm. **D–F** Unbiased relative counts of GFP-labeled OLs show significant deficits within all accessed cortical tissues (**D**) and differentially between the perilesional cortex (**E**) and medial cortex (mCtx, **F**) from *PLP^{GFP}* mice and *DCC^{D1290N}*:*PLP^{GFP}* mice at 1 dpi ($n = 4$–5). Values represent mean ± SEM. Welsh's unpaired, two-tailed *t*-test. *$p < 0.05$. **$p < 0.01$.

primarily localized to NeuN-positive neurons, where Netrin-1 was observed in both neuronal cell bodies (Fig. 1N–P) and axons (Fig. 1L) that make up the corpus callosum (CC) and other white matter structures. At 1 dpi (Fig. 1M, Q, R), tissue damage is observed in the injury epicenter and peri-lesional tissues (outline with white dotted line in Fig. 1Q, R). Neuronal losses in the injury epicenter led to a clear absence of netrin-1 expression in axons that resided in the CC (Fig. 1M arrowheads). We also observed a significant reduction of netrin-1 expression in peri-lesional tissues (Fig. 1R) preceding extensive neuronal cell loss at 1 dpi (Fig. 1Q). This region will eventually undergo both cell and tissue loss where only mCtx tissues remain by 7 dpi (Fig. S3A). The mCtx was defined as cortical tissue between the longitudinal fissure and apex of the CC (Fig. 1L Arrow). Cell loss in the mCtx continues throughout the first week post-injury but to a lesser extent. Together, these findings support a DepR environment following brain trauma, where CCI injury leads to increased DCC levels but not netrin-1 in perilesional tissues.

DCC receptor cleavage exacerbates OL cell death in peri-lesional tissues of the CCI injured brain

To examine whether DCC receptors contributed to OL cell death through DepR mechanisms, we took advantage of a *DCC*^{D1290N} receptor knock-in mouse, where the aspartate at position 1290 is replaced by an asparagine that results in a non-cleavable DCC receptor [34, 62]. *DCC*^{D1290N} mice were crossed with a myelin proteolipid protein (PLP)-promoter, GFP-reporter mouse line (*DCC*^{D1290N}:*PLP*^{GFP}) to examine OL cell numbers (Fig. 2). OL cell numbers were unbiasedly measured in peri-lesional cortex (Fig. 2E), mCtx (Fig. 2F), and combined (Fig. 2D) at 1 dpi as compared to sham controls. Sham tissue used longitudinal fissure to the apex of the CC for mCtx and apex of the CC to 2.3 mm from longitudinal fissure for tissues that corresponded to perilesional regions.

In cortical tissues, we observed reduced OL loss in *DCC*^{D1290N}:*PLP*^{GFP} mice relative to control *PLP*^{GFP} mice (Fig. 2). In particular, CCI injured *PLP*^{GFP} mice showed a significant ~38% decrease in OL survival (419 ± 56 cells, $n = 5$) from sham mice (672 ± 49 cells, $n = 4$) in spared cortical tissues, whereas injured *DCC*^{D1290N}:*PLP*^{GFP} mice exhibited only ~12% reduction at 1 dpi (654 ± 74 cells, $n = 5$) compared to sham controls (739 ± 85 cells, $n = 4$) (Fig. 2D). Given the differences in netrin-1 expression between perilesional and mCtx tissues, we also quantified OL numbers separately. In perilesional tissues, CCI injured *PLP*^{GFP} mice showed a significant ~56% decrease in OL survival (116 ± 21 cells, $n = 5$) from sham mice (261 ± 26 cells, $n = 4$), whereas the *DCC*^{D1290N}:*PLP*^{GFP} mice exhibited a ~30% reduction (202 ± 32 cells, $n = 5$) compared to sham mice (287 ± 57 cells, $n = 4$) (Fig. 2E). Similar non-significant trends were observed in the mCtx between *PLP*^{GFP} and *DCC*^{D1290N}:*PLP*^{GFP} mice at 1 dpi (Fig. 2F). Consistent with variable cell numbers observed between *PLP*^{GFP} and *DCC*^{D1290N}:*PLP*^{GFP} mice at 1 dpi, we also observed similar differences in spared tissues corresponding to mCtx and adjacent perilesional tissues (Fig. S3).

We also performed analysis at 7 dpi where only the mCtx remains (Fig. S4A). It should be noted that over the first week post-injury many additional secondary pathological events occur, including inflammatory responses and other DepR-mediated cell losses, that may further influence cell survival. Analysis of the mCtx, CC, and external capsule showed significant ~40–50% loss of OLs in CCI injured *PLP*^{GFP} mice, whereas non-significant reductions between ~20 and 30% were maintained in *DCC*^{D1290N}:*PLP*^{GFP} mice at 7 dpi (Fig. S4B–D). Given the partial sparing of OLs in the *DCC* mutant mice, we wondered whether there would also be greater neuronal survival after CCI injury. We observed a non-significant ~20% and ~14% reduction in NeuN^{+} cells in the mCtx *PLP*^{GFP} and *DCC*^{D1290N}:*PLP*^{GFP} mice at 7 dpi, respectively (Fig. S4E). Together, these observations support the role of DCC-mediated cell death in OLs in the adult mouse forebrain after CCI injury.

DCC^{D1290N} mutant mice show increased tissue sparing and reduced demyelination after CCI injury

To determine whether alterations in OL survival lead to improved tissue sparing and myelination, we examined the amount of preserved cortical tissue and the amount of myelin in *PLP*^{GFP} and *DCC*^{D1290N}:*PLP*^{GFP} mice at 7 dpi (Fig. 3). Gross differences in tissue sparing were observed between genotypes, where *DCC*^{D1290N}:*PLP*^{GFP} mice showed noticeably more spared cortical tissues (Fig. 3A–D). Unbiased stereological quantification of spared cortical tissues showed a significant ~37% loss of cortical volume among CCI injured *PLP*^{GFP} (6.3 ± 0.2 mm^3, $n = 13$) as compared to sham mice (10.0 ± 0.3 mm^3, $n = 5$) (Fig. 3E). No significant differences were observed in CCI injured *DCC*^{D1290N}:*PLP*^{GFP} (7.5 ± 0.4 mm^3, $n = 13$) compared to sham mice (9.4 ± 0.5 mm^3, $n = 5$) (Fig. 3E).

Demyelination is commonly associated with TBI pathology and may directly correspond to changes in OL survival. Thus, we also examined whether *DCC*^{D1290N}:*PLP*^{GFP} mice had increased myelin sparing after CCI injury. We employed an aurohalophosphate complex, Black Gold II [69] (Fig. 3). Densitometry analysis of staining intensity of CCI injured *PLP*^{GFP} mice showed a significant ~41% loss of myelin (Fig. 3J) in injured CC tract and external capsule (0.6 ± 0.07, $n = 9$) (Fig. 3B, G) as compared to sham mice (1.0 ± 0.03, $n = 8$) (Fig. 3A, F). Conversely, we observed no significant difference in myelin staining (Fig. 3J) between CCI injured *DCC*^{D1290N}:*PLP*^{GFP} mice (0.97 ± 0.08, $n = 7$) (Fig. 3D,I) and sham mice (1.02 ± 0.02, $n = 6$) (Fig. 3C,H). Together, these findings suggest that DCC cleavage plays a critical role in tissue damage, including large white matter tracts that associate with OL survival.

DCC^{D1290N} mutant mice show improved locomotor activity after CCI injury

To determine whether increased tissue sparing of the motor cortex led to improved locomotor function, we examined *PLP*^{GFP} and *DCC*^{D1290N}:*PLP*^{GFP} mice for motor activity using rotarod and wire hanging assessments (Fig. 4). *PLP*^{GFP} mice stayed on the rotating rod after training for an average of 55.4 ± 3.8 s prior to surgery (baseline, $n = 18$), which did not change in sham mice at 6 days post-surgery (Fig. 4A). Mice receiving a CCI injury showed a significantly reduced average of 27.2 ± 5.5 s at 6 dpi (Fig. 4A). *DCC*^{D1290N}:*PLP*^{GFP} mice stayed on the rotating rod for an average of 74.1 ± 7.9 s following pre-surgical training, which did not significantly change after CCI injury (64.5 ± 11.8 s) at 6 dpi ($n = 9$) (Fig. 4B). Figure 4C depicts these values normalized to baseline, where *PLP*^{GFP} CCI injured mice showed a ~51% reduction in latency on the rotating rod as compared to *PLP*^{GFP} sham mice, while *DCC*^{D1290N}:*PLP*^{GFP} sham and CCI injured mice showed no significant difference. We observed significantly greater ability of *DCC*^{D1290N}:*PLP*^{GFP} CCI mice to maintain balance on the rotating rod as compared to *PLP*^{GFP} CCI mice.

For wire hanging test, *PLP*^{GFP} mice were able to hang on the wire rod for an average of 67.6 ± 7.6 s prior to surgery (baseline) that significantly improved to 82.3 ± 14.1 s in sham mice ($n = 9$), which may reflect learned behavior (Fig. 4D). At 6 dpi, the latency was significantly reduced ~38% in the *PLP*^{GFP} CCI injured mice as compared to sham mice ($n = 11$) (Fig. 4D). This deficit was not observed in the *DCC*^{D1290N}:*PLP*^{GFP} CCI injured mice (Fig. 4E). Normalization to baseline showed a significant ~57% impairment in motor function in CCI injured *PLP*^{GFP} mice at 6 dpi, while CCI injured *DCC*^{D1290N}:*PLP*^{GFP} mice were reduced ~40% at 6 dpi compared to sham mice (Fig. 4F). Together, these motor behavior findings are suggestive that the functional improvement observed in non-cleavable *DCC*^{D1290N} mice correlate to improvements in tissue sparing and OL survival.

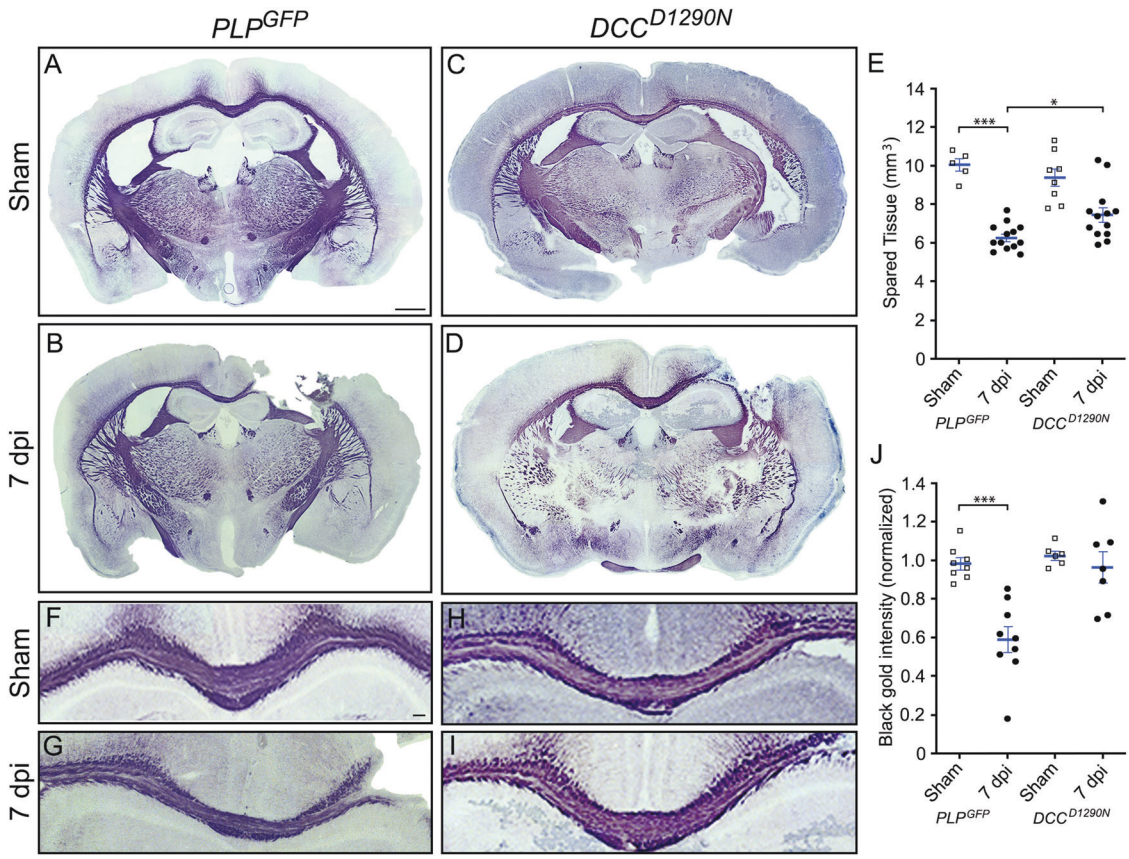

Fig. 3 ***DCC^{D1290N}*** **mice have improved cortical sparing and myelination after CCI injury. A–D** Representative coronal images showing Black Gold II myelin stain of sham controls (**A**,**C**) and 7 dpi (**B**,**D**) from *PLP^{GFP}* (**A**, **B**) and *DCC^{D1290N}*:*PLP^{GFP}* mice (**C**, **D**). **E** Quantification of cortical spared tissue (mm^3) in sham and 7 dpi from *PLP^{GFP}* mice and *DCC^{D1290N}*:*PLP^{GFP}* mice ($n = 5$–13). Magnified Black Gold II myelin stain of the CC of sham controls (**F**, **H**) and 7 dpi (**G**, **I**) from *PLP^{GFP}* (**F**, **G**) and *DCC^{D1290N}*:*PLP^{GFP}* mice (**H**, **I**). **J** Quantification of Black Gold II intensity within the CC of sham and 7 dpi *PLP^{GFP}* mice and *DCC^{D1290N}*:*PLP^{GFP}* mice. Values represent mean ± SEM. Two-way ANOVA with Tukey's post hoc comparison. *** $p < 0.001$.

DISCUSSION

Each year a significant number of people are hospitalized because of brain trauma with an array of pathophysiological deficits that may lead to severe and lasting cognitive dysfunction [4, 9, 10, 70, 71]. Cell and tissue losses are hallmarks of the secondary insult associated with severe traumatic brain injury (TBI), where both neurons and OLs are highly susceptible. Because OLs produce and maintain myelin sheaths, they are crucial in supporting axonal health and conductance in the CNS [72–75]. In fact, it is estimated that OLs have the highest metabolic rate of any cell type in the brain [76, 77]. This high energy demand makes them especially vulnerable to damage and cell death within a few hours after brain injury, which can persist for days in murine TBI models [12]. In humans, traumatic response can have long-term consequences where damaged white matter tracts have been observed for 18 years or more after a single injury [8]. Our findings uncover a novel role for the netrin-1 and DCC receptors in promoting OL cell loss after TBI. Here, we show that DCC receptors are highly enriched in OLs, resulting in dependence receptor (DepR)-mediated cell death in tissues containing low netrin-1 expression after CCI injury (Fig. 5). Netrin-1 administration is sufficient to block OL cell death. We exploited *DCC^{D1290N}* knock-in mice to genetically block proteolytic cleavage required for DepR-mediated apoptosis [34, 62], demonstrating that CCI injury leads to OL cell death through DepR mechanisms. Specifically, we observed reduced OL loss, greater myelin integrity, and improved motor function as compared to wild-type control mice, which is the first evidence that DCC regulates OL survival after TBI.

Traditional death receptors require ligand binding to initiate downstream signaling, whereas DepRs will initiate pro-death signaling in the absence of their ligand(s). DepRs are well-characterized in cancer biology fields, where they promote cell proliferation and survival [36, 38]. For example, the ephrin-B3 ligand encourages glioblastoma growth by repressing EphA4 DepR-mediated apoptosis [78]. But, DepRs have also been shown to function within the adult CNS, where ephrin-B3/EphA4 receptors can regulate adult neurogenesis by regulating neural progenitor cell death within the subventricular zone [79, 80]. EphB3 receptors have been linked to DepR mechanisms in the adult injured nervous system, where ephrin-B3/EphB3 mediated cell loss of cortical neurons [47], endothelial cells [48], and mature OLs [12, 45]. These findings demonstrate that cell death caused by TBI is closely associated with DepR mechanisms; however, these analyses have been limited to the ephrin/Eph family. Our analysis of DCC receptors provides support for an expanded role of DepR-mediated cell death after brain injury.

In the murine CCI model, the majority of OL cell death occurs within the first 24 h post-injury [12]. Therefore, a significant upregulation of the DCC receptor during this time period likely leads to an acute imbalance in the ligand-receptor ratio, supporting an environment for DepR-mediated OL cell death in the injured cortical penumbra. Netrin-1 is absent in perilesional tissues at 1 dpi, prior to the progressive cell death and tissue losses that will occur over the next few days. By 7 dpi the region designated as the medial cortex (mCtx) tissues will stabilize; although some OL cell death does occur, it is likely the result of

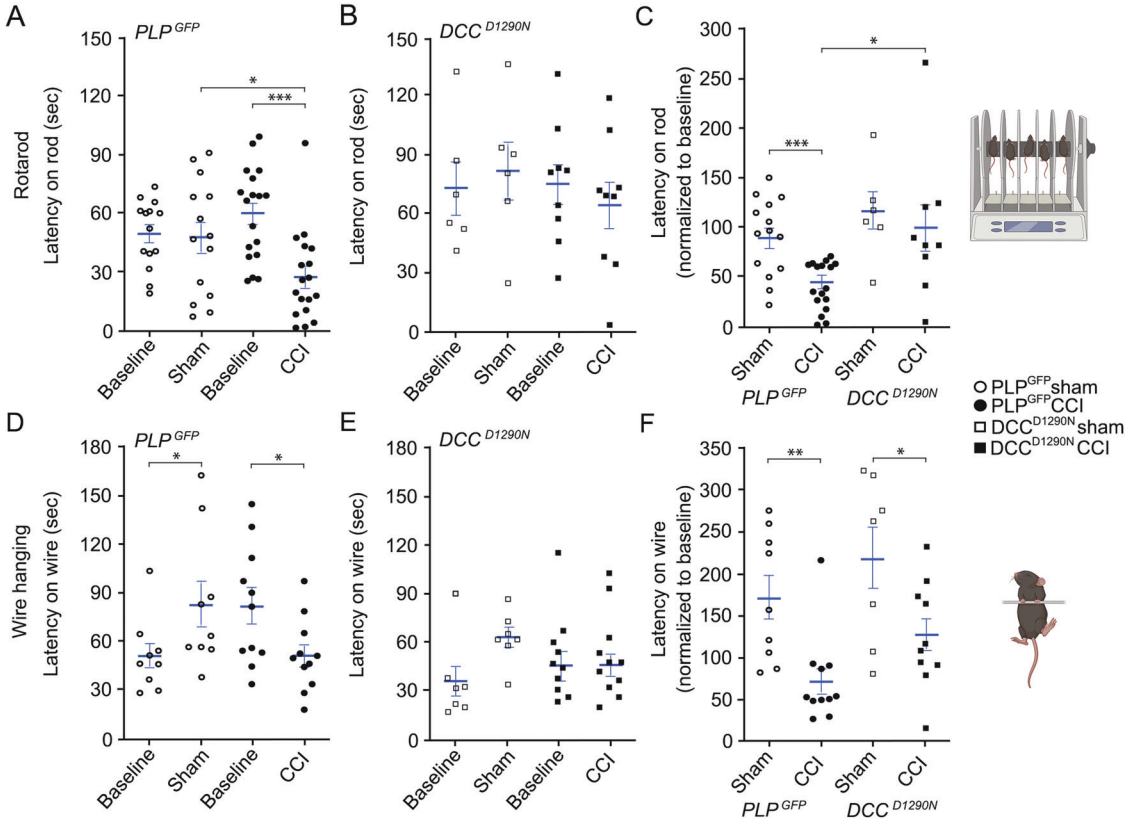

Fig. 4 ***DCC^{D1290N}* mice have improved locomotor function after CCI injury. A**,**B** Latency on the rotating rod for of sham (open) and CCI injured (closed) *PLP^{GFP}* (**A**) and *DCC^{D1290N}*:*PLP^{GFP}* (**B**) mice as compared to baseline. The latency to fall (seconds) was measured prior to surgery and at 6 dpi ($n = 6$–18). **C** Percent normalized time on the rod at 6 dpi relative to the baseline of each animal. **D**,**E** Wire hanging test of sham (open) and CCI injured (closed) *PLP^{GFP}* (**D**) and *DCC^{D1290N}*:*PLP^{GFP}* (**E**) mice as compared to baseline. The latency to fall (seconds) was measured prior to surgery and at 6 dpi ($n = 7$–11). **F** Percent normalized time on the wire at 6 dpi relative to the baseline of each animal. Values represent mean ± SEM. Repeated two-way ANOVA with Sidak's multiple comparison test, and Welsh's unpaired, two-tailed *t*-test. *$p < 0.05$.**$p < 0.01$. ***$p < 0.001$.

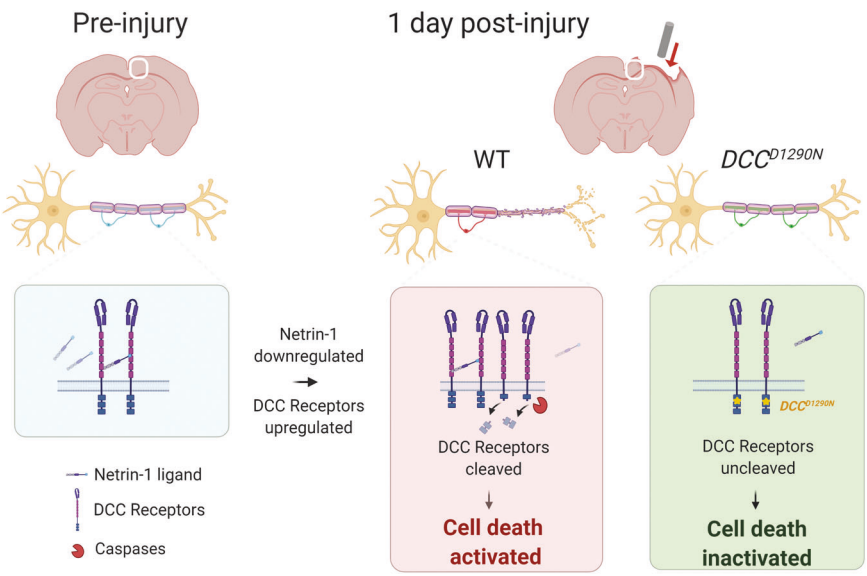

Fig. 5 Schematic model of Netrin-1/DCC receptor function in the injured brain. After cortical injury, DCC receptors are acutely upregulated while netrin-1 is downregulated in perilesional tissues, leading to a receptor-ligand imbalance. The DCC receptors without netrin-1 binding will undergo intracellular cleavage at the conserved aspartic acid residue at 1290, which leads to significant OL cell death. However, the knock-in DCC^{D1290N} point mutation blocks dependence receptor-mediated apoptosis, leading to greater cell survival, myelin integrity, and motor behavior after brain injury.

retained netrin-1 expression in mCtx tissues. Interestingly, netrin-1 levels are upregulated by 3 dpi, but mainly spared cortical tissues where little to no cell losses are observed. The previously described spatial-temporal differences in OL cell death in the cortex and underlying white matter tracts [12] support the delayed increase in netrin-1 expression, where most OLs in the injury epicenter and underlying white matter tract die prior to 3 dpi. It is also plausible that OLs express multiple DepRs (i.e., DCC and Eph receptors), suggesting that blocking cell death may require synergistic effects of their ligands. This is likely why we observed only partial blocking of OL cell death in the DCC^{D1290N} mice as compared to control PLP^{GFP} mice at 1 and 7 dpi, where trends are greater in cortical tissues than white matter tracts.

To differentiate the DepR role of DCC from other possible functions in the injured brain, we exploited DCC^{D1290N} mice, where the aspartic acid at position 1290 was mutated to asparagine. It has been well-documented that the *D1290N* mutation blocks caspase-dependent cleavage that is critical for conversion of DCC receptors to a pro-apoptotic death receptor [34, 62]. Thus, DCC^{D1290N} mice represent a novel approach to examining DCC pro-cell death mechanism without eliminating other DCC-mediated signaling pathways. We cannot rule out that DCC may have DepR functions in neurons, considering its neuronal expression [81–84] and has been shown to mediate neurodegeneration when netrin-1 is disengaged [41, 42, 59, 61]. We do observe a trend in greater neuronal survival in the CCI injured DCC^{D1290N} mice (Fig. S3); however, it remains to be determined whether this is a direct neuronal function and/or indirectly as a result of improved OL survival. This is further supported by our observation that neurons primarily produce netrin-1, which could function as an autocrine and/or paracrine for closely associated OLs. The close association between neurons and OLs, along with similar susceptibility to TBI-mediated cell death, support the dependence of DCC-expressing OLs on netrin-1-expressing neurons.

Targeting DCC DepR functions may represent an interesting therapeutic target for drug development, especially considering there are no clinical therapies to block tissue damage after TBI in humans. A recent study suggested that a novel netrin-1 derived peptide was neuroprotective after intracerebral hemorrhage in rodents [60]. In addition to TBI, dependence receptor mechanisms may be important for all CNS injuries (i.e., stroke or spinal cord injury) and neurodegenerative diseases (e.g., Alzheimer's disease, amyotrophic lateral sclerosis, multiple sclerosis, and Parkinson's disease), where DepRs may regulate cell death.

METHODS

Animals

Male *C57Bl6* (WT), DCC^{D1290N} [62], and PLP-green fluorescent protein (GFP) [85] mice were used for this study. All mice were between 2 and 4 months of age. Animals were kept under standard 12:12 light:dark cycles with food and water ad libitum. Animal procedures were approved by the University of Miami Animal Use and Care Committee. Control and injured groups consisted of littermates and were evaluated together when possible. Animal numbers were assessed by power analysis based on the effect size from previous studies. No animals were excluded from the study, and all experiments were run in at least duplicates.

OL cultures and viability assay

Primary OPCs were cultured from frozen stocks at a seeding density of 2×10^6 cells/well as previously described [45]. To produce mature OLs, the OPC medium was changed to DMEM with 1% gentamicin, 20 nM thyroid hormone (T3), and 10 ng/ml ciliary neurotrophic factor for 7–10 days. To induce cell death, 20 nM of staurosporine was administered to mature OLs for 48 h along with either the vehicle buffer or 4, 40, 400 ng/mL netrin-1 every 12 h over 2 days. Cell death was unbiasedly measured by the amount of Trypan Blue (#1450021, Bio-Rad, Hercules, CA, USA) using an automatic cell counter (TC20, Bio-Rad, Hercules, CA, USA). All in vitro experiments were repeated in triplicates.

Immunocytochemistry

Cells were fixed with 15% paraformaldehyde for 15 min, then subsequently blocked with 5% normal donkey serum for an hr. The following antibodies were used to label the cells overnight at 4 °C: rat α-PDGFRα 1:200 (#558774, BD Pharmingen, Franklin Lakes, NJ, USA), goat α-DCC 1:100 (#PA5-47951, ThermoFisher, Waltham, MA, USA), and rat α-MBP 1:500 (#MAB386, Millipore, Burlington, MA, USA). After washing the primary antibodies, secondary species-specific fluorescent antibodies Alexa Fluor-488 and Alexa Fluor-594 were applied at 1:300 (Invitrogen, Waltham, MA, USA). Representative images were acquired with a Zeiss Axiovert A1 fluorescence microscope.

scRNA analysis

Cell count matrices were obtained from Gene Expression Omnibus [86] with the series record GSE129609 [66]. The analyzed datasets were from isolated CNS tissue from six naive *B57Bl/6* male mice between 2 and 4 months old, where samples were processed according to the Drop-seq protocol [87] and sequenced on an Illumina NovaSeq 6000. Data was processed using Seurat (v.3.2) [88] in R (v.4.0.2) following the standard Seurat pipeline for log-normalization, dataset integration, principal component analysis, Uniform Manifold Approximation and Projection dimensional reduction, and differential gene expression analysis for each cluster against all other clusters. Cell-type specific gene transcripts to determine cell identity included, but were not limited to, *Tmem119*, *Siglech*, and *P2ry12* for microglia, *Aldh1l1*, *Aqp4*, and *Gfap* for astrocytes, and *Mog* and *Plp1* for OLs.

Controlled cortical impact (CCI) injury

Surgical procedures were as previously described [12, 47, 48, 89–91]. Briefly, animals were anaesthetized with ketamine (100 mg/kg) and xylazine (10 mg/kg) via an intraperitoneal injection. Littermates were randomly assigned to an experimental condition (CCI or sham). After a 5 mm craniotomy was performed over the right parieto-temporal cortex [−2.0 mm A/P and 2.0 mm lateral from bregma], a 3 mm bevelled piston controlled by an eCCI-6.3 apparatus (Custom Design & Fabrication, Sandston, VA, USA) was placed over the exposed dura. The CCI injury occurred at a velocity of 4 m/s with a depth of 0.55 mm and 150 ms impact dwell duration. The animals were closely monitored post-surgery and were individually housed for the remaining of the study. Sham littermate controls underwent the same surgical procedures except for the craniotomy and injury.

Flow cytometry

Sham and CCI injured WT mice were anaesthetized and transcardially perfused with 1× PBS (pH 7.4) at 1 day post injury (dpi). The underlying white matter tracts were discarded from the ipsilateral cortex to decrease the amount of myelin debris in the final cell suspension. The tissues were quickly and carefully dissected in cold HibernateA (without calcium) to maintain cell viability. The tissue was then enzymatically dissociated using a gentleMACS dissociator as per the manufacturer's protocol (Adult Brain Dissociation Kit for mouse and rat, Miltenyi Biotec #130-107-677, Bergisch Gladbach, Germany). Briefly, the dissociated tissue was strained through a 70 µm filter to remove any remaining clumps and pelleted at 300 g for 10 min at 4 °C. Myelin Debris Removal was conducted and the resulting cell suspension was centrifuged at 3000 *g* for 10 min at 4 °C. The cell pellet was washed with Flow Buffer composed of 0.5% bovine serum albumin (BSA; Sigma Aldrich, St. Louis, MO, USA) and 2 mM EDTA (pH7.2) in sterile 1× PBS. The cells were labeled with the following primary antibodies for an hour at 4 °C: CD45— PE/Cy7 (1:100, #103114, BioLegend, San Diego, CA, USA), CD11b— redFlour710 (1:50, #80-0114, Tonbo Biosciences, San Diego, CA, USA), ACSA-2—PE (1:50, #130-116-141, Miltenyi Biotec), O1— Alexa 647 (1:50, #51-6506-82, eBioscience, Waltham, MA, USA), Goat αDCC (1:50, #PA5-47951, ThermoFisher, Waltham, MA, USA). Cells were briefly washed with Flow Buffer before labeling with a Donkey αGoat Alexa 488 secondary antibody (1:50, Invitrogen #A11055) for 30 min at 4 °C. The samples were briefly washed again with Flow Buffer prior to adding DAPI for distinguishing viable cells (0.1 µg/mL; #130-111-570, Miltenyi Biotec). The cell suspensions were immediately analyzed with a MoFlo Astrios QE (Beckman Coulter, Brea, CA, USA). Flow cytometric gating was set based on fluorescent signal from unstained and single channel control samples: viable cells had low DAPI signal, microglia were $CD11b^{High}$ and $CD45^{Low}$ (macrophages were $CD45^{high}$), astrocytes were GFAP positive, and OLs were O1 expressing. The experimenters were blinded to the injury conditions during the flow cytometry protocol, gating, and analyses.

Western blot

Fresh ipsilateral cortices of sham or CCI injured WT male mice were collected at 2 hpi, 6 hpi, 24 hpi, 3 dpi, or 7 dpi. Lysates were prepared and ~40 µg were resolved in 4–20% gradient polyacrylamide gels (Criterion TGX Stain-Free, Bio-Rad, Hercules, CA, USA). Stain-Free activated gels underwent a semi-dry transfer for 7 min onto nitrocellulose membranes according to manufacturer's instructions (Trans-Blot Turbo Transfer System, Bio-Rad, Hercules, CA, USA). Membranes were immediately visualized to access total protein levels prior to blocking with 5% BSA for an hour at room temperature. The primary rabbit anti-Netrin-1 antibody (1:500, #ab126729, Abcam, Cambridge, UK) was applied overnight at 4 °C.

RNA isolation and RT-qPCR

Fresh ipsilateral cortices of sham or CCI injured WT male mice were collected for subsequent RNA extraction using the Direct-zol RNA miniprep kit (#R2051, Zymo Research, Irvine, CA, USA). All steps were completed according to the manufacturer's instructions. The RNA was reverse transcribed into cDNA using a High-Capacity cDNA reverse transcription kit (#4368814, ThermoFisher, Waltham, MA, USA) for RT-qPCR. qPCR was performed using AmpliTaq Gold 360 Master Mix (#4398881, ThermoFisher) with 50 nM ROX passive reference dye (#75768, ThermoFisher), a QuantStudio 3 Thermocycler (Applied Biosystems) using TaqMan for our gene of interest: *netrin-1* (Mm00500896_m1, Applied Biosystems). *Glyceraldehyde 3-phosphate dehydrogenase* (*Gapdh*, Mm99999915_g1, Applied Biosystems) was used as an endogenous control. The average Ct value for each duplicate was used. The ΔCt was subsequently calculated by subtracting the Ct_{gapdh} from its respective $Ct_{netrin\text{-}1}$. The ΔΔCt was normalized by subtracting the average ΔCt of sham samples from the ΔCt of CCI injured samples. The absence of RNA material was used as a negative control. Fold difference is equal to $2^{-(\Delta\Delta Ct)}$. All analyses were performed in a randomized non-biased manner using the QuantStudio Designer and Analysis software v1.5.1 (Applied Biosytems).

Netrin-1 immunoreactivity. Histological preparations and stereological counts were performed as described before [12, 45, 92]. In summary, WT, PLP^{GFP} and DCC^{D1290N}:PLP^{GFP} male mice were transcardially perfused with 1× PBS (pH 7.4) following cold 4% paraformaldehyde (pH 7.4) at 7 dpi. The brains were postfixed with additional 4% paraformaldehyde overnight at 4 °C, then transferred to 30% sucrose in PBS solution for 3 days at 4 °C. Brains were embedded in Tissue-TEK OCT solution (Sakura, Torrance, CA, USA) and flash frozen in isopentane. Tissues were serially cut every 30 µm using a cryostat (Leica, Buffalo Grove, IL, USA). Because netrin-1 requires antigen retrieval, sham and CCI injured tissues at 1 dpi were boiled in fresh sodium citrate buffer (10 mM sodium citrate, 0.05% Tween-20, pH 6.0) for 9 min. Sections were briefly rinsed with distilled water before blocking with 5% normal donkey serum in PBSGT (1× PBS, 0.2% gelatine, 0.25% TritonX-100) for 2 h at room temperature. Rabbit αNetrin-1 (1:400, #ab126729, Abcam, Cambridge, UK) and mouse αNeuN antibodies (1:400, #MAB377, Millipore, Burlington, MA, USA) were prepared in PBSGT and applied overnight at room temperature. Sections were washed 3× for 10 min in PBST (0.25% TritonX-100 in PBS) prior to incubating with their respective secondary antibodies for 2 h at room temperature (Donkey αmouse Alexa Fluor-488 and Donkey αrabbit Alexa Fluor-647 at 1:400; Invitrogen, Waltham, MA, USA). Sections were washed 3× for 10 min in PBST and mounted with Fluoro-Gel (#17985-10, E.M.S., Hatfield, PA, USA). Representative images were acquired with a 10× objective on a Dragonfly high speed confocal microscope (Oxford Instruments, Abingdon, England) every 2 µm at 2048 × 2048. Montages were stitched using the Imaris Stitcher software x64 (v9.8). All settings were maintained the same.

OL cell counts. OLs were detected by GFP fluorescence driven by the PLP promoter (PLP^{GFP}), and neurons were immunolabeled with αNeuN antibodies (1:300, #MAB377, Millipore, Burlington, MA, USA). Nonbiased cell counting was performed on 4 sections serially distanced 300 µm by means of the Imaris spot detection (v9.8.2), or the optical fractionator method and the optical dissector probe. For 1 dpi tissues, the mCtx and medial perilesional tissues were manually contoured from high resolution confocal z-stack images acquired from the Dragonfly microscope (Oxford Instruments, Abingdon, England) using a 10× objective at 1024 × 1024. All visible PLP^{GFP+} cells within these regions were counted using the Imaris semi-automated spot detection and manually reviewed by the same experimenter. For 7 dpi tissues, the mCtx, corpus collosum, and external capsule in the ipsilateral hemisphere (as highlighted in Fig. S3A) were manually contoured using a 5× objective on a motorized Olympus BX51TRF microscope, Optronix cooled camera, and MicroBrightField StereoInvestigator software package (MBF Bioscience, Williston, VT, USA). Finally, a grid of 175 × 175 μm^2 was placed over the selected contour where PLP^{GFP+} or $\alpha NeuN^{+}$ cells were counted at 63× in immersion oil (sampling box 50 × 50 μm^2 for the CC and 75 × 75 μm^2 for the cortex). Experimenters were blinded to the genotype and injury condition throughout the analyses.

Tissue sparing

To assess the amount of cortical tissue spared after injury, four tissue sections serially distanced at 300 µm each were selected for analysis. The ipsilateral cortical area was predefined before examining the tissues. The areas were contoured using NeuroLucida on a motorized Olympus BX51TRF microscope with a 5× objective. The tissue evaluation was performed in a blinded manner to the genotype and injury condition throughout the analyses.

Black-Gold II stain

White matter tracts were labeled with the myelin- specific Black-Gold II stain [69]. As per manufacturer's instructions (#TR-100-BG, Biosensis, Thebarton, Australia), fixed tissue sections were placed on 50 °C slide warmer for 30 min prior to hydrating the sections with distilled water. Tissue sections were incubated at 65 °C with pre-heated 1× Black-Gold II solution for ~9–12 min. The sections were washed with distilled water and incubated with the sodium thiosulfate solution for 3 min. Tissue sections were washed three times 5 min with distilled water before mounting with Fluoro-Gel (#17985-10, E.M.S., Hatfield, PA, USA). Slides were scanned with a PathScan Enabler (Meyer instruments, Houston, TX, USA). The Black Gold intensity within the ipsi- and contralateral CC and external capsule were measured using ImageJ. The Black-Gold intensity was normalized to the respective contralateral hemisphere within the same tissue section. The evaluator was blinded to the genotype and condition during staining and quantification.

RotaRod test

Motor function was assessed at 3 and 6 dpi using a RotaRod apparatus (#LE8205, Harvard Apparatus, Holliston, MA, USA) for mice, as previously described [47]. In summary, the initial velocity of 4 r.p.m. accelerated to 60 r.p.m. in 10 min. Training occurred for 3 days prior to surgery with four-trials each day (2 min rest period between each trial). The last day of training was considered baseline. The latency of each trial was measured until either the mouse fell off or passively gripped the rotating rod for a full turn. RotaRod was conducted during the same time of day to avoid potential circadian differences in motor performance. The evaluator was blinded to the genotype and condition.

Wire hanging test

Grip strength was assessed at 6 dpi via a wire hanging test. Briefly, the mice had to hang onto the 55 cm long metal wire rod for a maximum of 3 min. The mice had five-trials each day with a 1 min rest period between each trial. Initial training occurred just prior to surgery and the mice were assessed again at 6 dpi. The latency of each trial was recorded until either the mouse fell off or jumped off. Due to variability in motivation or due to fatigue, the longest 3 of 5 trials were averaged for statistical analyses. Wire hanging was conducted during the same time of day to avoid potential circadian differences in motor performance. The evaluator was blinded to the genotype and condition.

Statistical analysis

Prism software (version 8, GraphPad, San Diego, CA, USA) was used for statistical comparisons. Data were analyzed using a two-tailed unpaired Welsh *t*-test, or with a one- or two-way ANOVA with a Tukey's post hoc comparison. Alpha value was set to 0.05 for all analyses. The estimate of variance was similar between all groups. All graphs depict mean values with the standard error of mean (S.E.M.) for error bars.

DATA AVAILABILITY

The data analyzed during this study are included in this published paper and the supplemental data files. Additional supporting data are available from the corresponding authors upon reasonable request.

REFERENCES

1. Dewan MC, Rattani A, Gupta S, Baticulon RE, Hung YC, Punchak M, et al. Estimating the global incidence of traumatic brain injury. J Neurosurg. 2019;130:1080–97.
2. Daugherty J, Waltzman D, Sarmiento K, Xu L. Traumatic Brain Injury-Related Deaths by Race/Ethnicity, Sex, Intent, and Mechanism of Injury - United States, 2000-2017. MMWR Morb Mortal Wkly Rep. 2019;68:1050–6.
3. Vaishnavi S, Rao V, Fann JR. Neuropsychiatric problems after traumatic brain injury: unraveling the silent epidemic. Psychosomatics 2009;50:198–205.
4. McDonald S, Genova H. The effect of severe traumatic brain injury on social cognition, emotion regulation, and mood. Handb Clin Neurol. 2021;183:235–60.
5. Shah EJ, Gurdziel K, Ruden DM. Mammalian Models of Traumatic Brain Injury and a Place for Drosophila in TBI Research. Front Neurosci. 2019;13:409.
6. Aravind A, Ravula AR, Chandra N, Pfister BJ. Behavioral Deficits in Animal Models of Blast Traumatic Brain Injury. Front Neurol. 2020;11:990.
7. Shultz SR, McDonald SJ, Corrigan F, Semple BD, Salberg S, Zamani A, et al. Clinical Relevance of Behavior Testing in Animal Models of Traumatic Brain Injury. J Neurotrauma. 2020;37:2381–400.
8. Johnson VE, Stewart JE, Begbie FD, Trojanowski JQ, Smith DH, Stewart W. Inflammation and white matter degeneration persist for years after a single traumatic brain injury. Brain 2013;136:28–42.
9. Johnson VE, Stewart W, Smith DH. Axonal pathology in traumatic brain injury. Exp Neurol. 2013;246:35–43.
10. Filley CM, Kelly JP. White Matter and Cognition in Traumatic Brain Injury. J Alzheimers Dis. 2018;65:345–62.
11. Flygt J, Gumucio A, Ingelsson M, Skoglund K, Holm J, Alafuzoff I, et al. Human Traumatic Brain Injury Results in Oligodendrocyte Death and Increases the Number of Oligodendrocyte Progenitor Cells. J Neuropathol Exp Neurol. 2016;75:503–15.
12. Tsenkina Y, Tapanes SA, Díaz MM, Titus DJ, Gajavelli S, Bullock R, et al. EphB3 interacts with initiator caspases and FHL-2 to activate dependence receptor cell death in oligodendrocytes after brain injury. Brain Commun 2020;2:fcaa175.
13. Bramlett HM, Dietrich WD. Quantitative structural changes in white and gray matter 1 year following traumatic brain injury in rats. Acta Neuropathol. 2002;103:607–14.
14. Flygt J, Djupsjö A, Lenne F, Marklund N. Myelin loss and oligodendrocyte pathology in white matter tracts following traumatic brain injury in the rat. Eur J Neurosci. 2013;38:2153–65.
15. Sullivan GM, Mierzwa AJ, Kijpaisalratana N, Tang H, Wang Y, Song SK, et al. Oligodendrocyte lineage and subventricular zone response to traumatic axonal injury in the corpus callosum. J Neuropathol Exp Neurol. 2013;72:1106–25.
16. Mierzwa AJ, Marion CM, Sullivan GM, McDaniel DP, Armstrong RC. Components of myelin damage and repair in the progression of white matter pathology after mild traumatic brain injury. J Neuropathol Exp Neurol. 2015;74:218–32.
17. Marion CM, Radomski KL, Cramer NP, Galdzicki Z, Armstrong RC. Experimental Traumatic Brain Injury Identifies Distinct Early and Late Phase Axonal Conduction Deficits of White Matter Pathophysiology, and Reveals Intervening Recovery. J Neurosci. 2018;38:8723–36.
18. Ashkenazi A, Dixit VM. Death receptors: signaling and modulation. Science 1998;281:1305–8.
19. Knoblach SM, Fan L, Faden AI. Early neuronal expression of tumor necrosis factor-alpha after experimental brain injury contributes to neurological impairment. J Neuroimmunol. 1999;95:115–25.
20. Beer R, Franz G, Schöpf M, Reindl M, Zelger B, Schmutzhard E, et al. Expression of Fas and Fas ligand after experimental traumatic brain injury in the rat. J Cereb Blood Flow Metab. 2000;20:669–77.
21. Qiu J, Whalen MJ, Lowenstein P, Fiskum G, Fahy B, Darwish R, et al. Upregulation of the Fas receptor death-inducing signaling complex after traumatic brain injury in mice and humans. J Neurosci. 2002;22:3504–11.
22. Zhang X, Graham SH, Kochanek PM, Marion DW, Nathaniel PD, Watkins SC, et al. Caspase-8 expression and proteolysis in human brain after severe head injury. Faseb J. 2003;17:1367–9.
23. Lotocki G, Alonso OF, Dietrich WD, Keane RW. Tumor necrosis factor receptor 1 and its signaling intermediates are recruited to lipid rafts in the traumatized brain. J Neurosci. 2004;24:11010–6.
24. Raghupathi R. Cell death mechanisms following traumatic brain injury. Brain Pathol. 2004;14:215–22.
25. Bermpohl D, You Z, Lo EH, Kim HH, Whalen MJ. TNF alpha and Fas mediate tissue damage and functional outcome after traumatic brain injury in mice. J Cereb Blood Flow Metab. 2007;27:1806–18.
26. Shohami E, Ginis I, Hallenbeck JM. Dual role of tumor necrosis factor alpha in brain injury. Cytokine Growth Factor Rev. 1999;10:119–30.
27. Narayan RK, Michel ME, Ansell B, Baethmann A, Biegon A, Bracken MB, et al. Clinical trials in head injury. J Neurotrauma. 2002;19:503–57.
28. Xiong Y, Mahmood A, Chopp M. Emerging treatments for traumatic brain injury. Expert Opin Emerg Drugs. 2009;14:67–84.
29. Loane DJ, Faden AI. Neuroprotection for traumatic brain injury: translational challenges and emerging therapeutic strategies. Trends Pharm Sci. 2010; 31:596–604.
30. Kabadi SV, Faden AI. Neuroprotective strategies for traumatic brain injury: improving clinical translation. Int J Mol Sci. 2014;15:1216–36.
31. Dang B, Chen W, He W, Chen G. Rehabilitation Treatment and Progress of Traumatic Brain Injury Dysfunction. Neural Plast. 2017;2017:1582182.
32. Rana A, Singh S, Sharma R, Kumar A. Traumatic Brain Injury Altered Normal Brain Signaling Pathways: Implications for Novel Therapeutics Approaches. Curr Neuropharmacol. 2019;17:614–29.
33. Bonilla C, Zurita M. Cell-Based Therapies for Traumatic Brain Injury: Therapeutic Treatments and Clinical Trials. Biomedicines. 2021;9:669.
34. Mehlen P, Rabizadeh S, Snipas SJ, Assa-Munt N, Salvesen GS, Bredesen DE. The DCC gene product induces apoptosis by a mechanism requiring receptor proteolysis. Nature 1998;395:801–4.
35. Rodrigues S, De Wever O, Bruyneel E, Rooney RJ, Gespach C. Opposing roles of netrin-1 and the dependence receptor DCC in cancer cell invasion, tumor growth and metastasis. Oncogene 2007;26:5615–25.
36. Mehlen P, Guenebeaud C. Netrin-1 and its dependence receptors as original targets for cancer therapy. Curr Opin Oncol. 2010;22:46–54.
37. Krimpenfort P, Song JY, Proost N, Zevenhoven J, Jonkers J, Berns A. Deleted in colorectal carcinoma suppresses metastasis in p53-deficient mammary tumours. Nature 2012;482:538–41.
38. Goldschneider D, Mehlen P. Dependence receptors: a new paradigm in cell signaling and cancer therapy. Oncogene 2010;29:1865–82.
39. Wu S, Guo X, Zhou J, Zhu X, Chen H, Zhang K, et al. High expression of UNC5B enhances tumor proliferation, increases metastasis, and worsens prognosis in breast cancer. Aging (Albany NY). 2020;12:17079–98.
40. Lourenço FC, Galvan V, Fombonne J, Corset V, Llambi F, Müller U, et al. Netrin-1 interacts with amyloid precursor protein and regulates amyloid-beta production. Cell Death Differ. 2009;16:655–63.
41. Chen G, Kang SS, Wang Z, Ahn EH, Xia Y, Liu X, et al. Netrin-1 receptor UNC5C cleavage by active δ-secretase enhances neurodegeneration, promoting Alzheimer's disease pathologies. Sci Adv. 2021;7:eabe4499.
42. Jasmin M, Ahn EH, Voutilainen MH, Fombonne J, Guix C, Viljakainen T, et al. Netrin-1 and its receptor DCC modulate survival and death of dopamine neurons and Parkinson's disease features. Embo J. 2021;40:e105537.
43. Wetzel-Smith MK, Hunkapiller J, Bhangale TR, Srinivasan K, Maloney JA, Atwal JK, et al. A rare mutation in UNC5C predisposes to late-onset Alzheimer's disease and increases neuronal cell death. Nat Med. 2014;20:1452–7.
44. Qu Y, Zhao J, Wang Y, Gao Z. Silencing ephrinB3 improves functional recovery following spinal cord injury. Mol Med Rep. 2014;9:1761–6.
45. Tsenkina Y, Ricard J, Runko E, Quiala-Acosta MM, Mier J, Liebl DJ. EphB3 receptors function as dependence receptors to mediate oligodendrocyte cell death following contusive spinal cord injury. Cell Death Dis. 2015;6:e1922.
46. Theus MH, Ricard J, Bethea JR, Liebl DJ. EphB3 limits the expansion of neural progenitor cells in the subventricular zone by regulating p53 during homeostasis and following traumatic brain injury. Stem Cells. 2010;28:1231–42.
47. Theus MH, Ricard J, Glass SJ, Travieso LG, Liebl DJ. EphrinB3 blocks EphB3 dependence receptor functions to prevent cell death following traumatic brain injury. Cell Death Dis. 2014;5:e1207.
48. Assis-Nascimento P, Tsenkina Y, Liebl DJ. EphB3 signaling induces cortical endothelial cell death and disrupts the blood-brain barrier after traumatic brain injury. Cell Death Dis. 2018;9:7.
49. Mehlen P, Thibert C. Dependence receptors: between life and death. Cell Mol Life Sci. 2004;61:1854–66.
50. Keino-Masu K, Masu M, Hinck L, Leonardo ED, Chan SS, Culotti JG, et al. Deleted in Colorectal Cancer (DCC) encodes a netrin receptor. Cell 1996;87:175–85.
51. Llambi F, Causeret F, Bloch-Gallego E, Mehlen P. Netrin-1 acts as a survival factor via its receptors UNC5H and DCC. Embo J. 2001;20:2715–22.
52. Finci LI, Krüger N, Sun X, Zhang J, Chegkazi M, Wu Y, et al. The crystal structure of netrin-1 in complex with DCC reveals the bifunctionality of netrin-1 as a guidance cue. Neuron 2014;83:839–49.
53. Finger JH, Bronson RT, Harris B, Johnson K, Przyborski SA, Ackerman SL. The netrin 1 receptors Unc5h3 and Dcc are necessary at multiple choice points for the guidance of corticospinal tract axons. J Neurosci. 2002;22:10346–56.
54. Forcet C, Stein E, Pays L, Corset V, Llambi F, Tessier-Lavigne M, et al. Netrin-1-mediated axon outgrowth requires deleted in colorectal cancer-dependent MAPK activation. Nature 2002;417:443–7.
55. Jarjour AA, Bull SJ, Almasieh M, Rajasekharan S, Baker KA, Mui J, et al. Maintenance of axo-oligodendroglial paranodal junctions requires DCC and netrin-1. J Neurosci. 2008;28:11003–14.
56. Rajasekharan S, Baker KA, Horn KE, Jarjour AA, Antel JP, Kennedy TE. Netrin 1 and Dcc regulate oligodendrocyte process branching and membrane extension via Fyn and RhoA. Development 2009;136:415–26.

57. Mehlen P, Mazelin L. The dependence receptors DCC and UNC5H as a link between neuronal guidance and survival. Biol Cell. 2003;95:425–36.
58. Furne C, Rama N, Corset V, Chédotal A, Mehlen P. Netrin-1 is a survival factor during commissural neuron navigation. Proc Natl Acad Sci. 2008;105:14465–70.
59. Chen J, Du H, Zhang Y, Chen H, Zheng M, Lin P, et al. Netrin-1 Prevents Rat Primary Cortical Neurons from Apoptosis via the DCC/ERK Pathway. Front Cell Neurosci. 2017;11:387.
60. Liu L, Liu KJ, Cao JB, Yang J, Yu HL, He XX, et al. A Novel Netrin-1-Derived Peptide Enhances Protection against Neuronal Death and Mitigates of Intracerebral Hemorrhage in Mice. Int J Mol Sci. 2021;22:4829.
61. Furne C, Corset V, Hérincs Z, Cahuzac N, Hueber A-O, Mehlen P. The dependence receptor DCC requires lipid raft localization for cell death signaling. Proc Natl Acad Sci USA. 2006;103:4128–33.
62. Castets M, Broutier L, Molin Y, Brevet M, Chazot G, Gadot N, et al. DCC constrains tumour progression via its dependence receptor activity. Nature 2011;482:534–7.
63. Broutier L, Creveaux M, Vial J, Tortereau A, Delcros JG, Chazot G, et al. Targeting netrin-1/DCC interaction in diffuse large B-cell and mantle cell lymphomas. EMBO Mol Med. 2016;8:96–104.
64. Boussouar A, Tortereau A, Manceau A, Paradisi A, Gadot N, Vial J, et al. Netrin-1 and Its Receptor DCC Are Causally Implicated in Melanoma Progression. Cancer Res. 2020;80:747–56.
65. Mehlen P, Bredesen DE. The dependence receptor hypothesis. Apoptosis 2004;9:37–49.
66. Wheeler MA, Clark IC, Tjon EC, Li Z, Zandee SEJ, Couturier CP, et al. MAFG-driven astrocytes promote CNS inflammation. Nature 2020;578:593–9.
67. Assis-Nascimento P, Umland O, Cepero ML, Liebl DJ. A flow cytometric approach to analyzing mature and progenitor endothelial cells following traumatic brain injury. J Neurosci Methods. 2016;263:57–67.
68. Kennedy TE, Serafini T, de la Torre JR, Tessier-Lavigne M. Netrins are diffusible chemotropic factors for commissural axons in the embryonic spinal cord. Cell 1994;78:425–35.
69. Schmued L, Bowyer J, Cozart M, Heard D, Binienda Z, Paule M. Introducing Black-Gold II, a highly soluble gold phosphate complex with several unique advantages for the histochemical localization of myelin. Brain Res. 2008;1229:210–7.
70. Wood RL. Accelerated cognitive aging following severe traumatic brain injury: A review. Brain Inj. 2017;31:1270–8.
71. Wu D, Kumal JPP, Lu X, Li Y, Mao D, Tang X, et al. Traumatic Brain Injury Accelerates the Onset of Cognitive Dysfunction and Aggravates Alzheimer's-Like Pathology in the Hippocampus by Altering the Phenotype of Microglia in the APP/PS1 Mouse Model. Front Neurol. 2021;12:666430.
72. Klugmann M, Schwab MH, Pühlhofer A, Schneider A, Zimmermann F, Griffiths IR, et al. Assembly of CNS myelin in the absence of proteolipid protein. Neuron 1997;18:59–70.
73. Griffiths I, Klugmann M, Anderson T, Yool D, Thomson C, Schwab MH, et al. Axonal swellings and degeneration in mice lacking the major proteolipid of myelin. Science 1998;280:1610–3.
74. Fünfschilling U, Supplie LM, Mahad D, Boretius S, Saab AS, Edgar J, et al. Glycolytic oligodendrocytes maintain myelin and long-term axonal integrity. Nature 2012;485:517–21.
75. Duncan GJ, Simkins TJ, Emery B. Neuron-Oligodendrocyte Interactions in the Structure and Integrity of Axons. Front Cell Dev Biol. 2021;9:653101.
76. Harris JJ, Attwell D. The energetics of CNS white matter. J Neurosci. 2012;32:356–71.
77. Rosko L, Smith VN, Yamazaki R, Huang JK. Oligodendrocyte Bioenergetics in Health and Disease. Neuroscientist 2019;25:334–43.
78. Royet A, Broutier L, Coissieux MM, Malleval C, Gadot N, Maillet D, et al. Ephrin-B3 supports glioblastoma growth by inhibiting apoptosis induced by the dependence receptor EphA4. Oncotarget 2017;8:23750–9.
79. Ricard J, Salinas J, Garcia L, Liebl DJ. EphrinB3 regulates cell proliferation and survival in adult neurogenesis. Mol Cell Neurosci. 2006;31:713–22.
80. Furne C, Ricard J, Cabrera JR, Pays L, Bethea JR, Mehlen P, et al. EphrinB3 is an anti-apoptotic ligand that inhibits the dependence receptor functions of EphA4 receptors during adult neurogenesis. Biochim Biophys Acta. 2009;1793:231–8.
81. Manitt C, Colicos MA, Thompson KM, Rousselle E, Peterson AC, Kennedy TE. Widespread expression of netrin-1 by neurons and oligodendrocytes in the adult mammalian spinal cord. J Neurosci. 2001;21:3911–22.
82. Hérincs Z, Corset V, Cahuzac N, Furne C, Castellani V, Hueber AO, et al. DCC association with lipid rafts is required for netrin-1-mediated axon guidance. J Cell Sci. 2005;118:1687–92.
83. Goldman JS, Ashour MA, Magdesian MH, Tritsch NX, Harris SN, Christofi N, et al. Netrin-1 promotes excitatory synaptogenesis between cortical neurons by initiating synapse assembly. J Neurosci. 2013;33:17278–89.
84. Horn KE, Glasgow SD, Gobert D, Bull SJ, Luk T, Girgis J, et al. DCC expression by neurons regulates synaptic plasticity in the adult brain. Cell Rep. 2013;3:173–85.
85. Fuss B, Mallon B, Phan T, Ohlemeyer C, Kirchhoff F, Nishiyama A, et al. Purification and analysis of in vivo-differentiated oligodendrocytes expressing the green fluorescent protein. Dev Biol. 2000;218:259–74.
86. James SL, Theadom A, Ellenbogen RG, Bannick MS, Montjoy-Venning W, Lucchesi LR, et al. Global, regional, and national burden of traumatic brain injury and spinal cord injury, 1990–2016: a systematic analysis for the Global Burden of Disease Study 2016. Lancet Neurol. 2019;18:56–87.
87. Macosko EZ, Basu A, Satija R, Nemesh J, Shekhar K, Goldman M, et al. Highly Parallel Genome-wide Expression Profiling of Individual Cells Using Nanoliter Droplets. Cell 2015;161:1202–14.
88. Stuart T, Butler A, Hoffman P, Hafemeister C, Papalexi E, Mauck WM 3rd, et al. Comprehensive Integration of Single-Cell Data. Cell 2019;177:1888–902. e21
89. Dixon KJ, Mier J, Gajavelli S, Turbic A, Bullock R, Turnley AM, et al. EphrinB3 restricts endogenous neural stem cell migration after traumatic brain injury. Stem Cell Res. 2016;17:504–13.
90. Perez EJ, Cepero ML, Perez SU, Coyle JT, Sick TJ, Liebl DJ. EphB3 signaling propagates synaptic dysfunction in the traumatic injured brain. Neurobiol Dis. 2016;94:73–84.
91. Perez EJ, Tapanes SA, Loris ZB, Balu DT, Sick TJ, Coyle JT, et al. Enhanced astrocytic d-serine underlies synaptic damage after traumatic brain injury. J Clin Investig. 2017;127:3114–25.
92. Vazquez-Rosa E, Watson MR, Sahn JJ, Hodges TR, Schroeder RE, Cintron-Perez CJ, et al. Neuroprotective Efficacy of a Sigma 2 Receptor/TMEM97 Modulator (DKR-1677) after Traumatic Brain Injury. ACS Chem Neurosci. 2019;10:1595–602.

ACKNOWLEDGEMENTS

The authors thank Maria L. Cepero, Maria M Quiala-Acosta, and Jose Mier for technical assistance and animal husbandry. Dr Oliver Umland was instrumental in the flow cytometry gating and analysis. We thank Drs Haritha Desu and Roberta Brambilla for reagents and guidance. Lastly, we thank Dr Pantelis Tsoulfas and Yan Shi for microscopy support. Graphical model was created in Biorender.com.

AUTHOR CONTRIBUTIONS

PM, DJL, and YT conceived the study. PM provided technical and material support. MMD, YT, DA, DJL, and PM provided acquisition, analysis, interpretation of data, and statistical analysis. MMD and DJL drafted the paper. All authors read and approved the paper.

FUNDING

This work was supported by the Miami Project to Cure Paralysis, National Institute of Health/National Institute of Neurological Disorders and Stroke (NS098740, NS120028), Foundation Bettencourt (PM), ANR (PM) and ligue contre le cancer (PM), and the Lois Pope Life Foundation.

COMPETING INTERESTS

The authors declare no competing interests.

ETHICS APPROVAL

Animal procedures were approved by the University of Miami Animal Use and Care Committee. No human subjects were involved in this study.

ADDITIONAL INFORMATION

Supplementary information The online version contains supplementary material available at https://doi.org/10.1038/s41418-022-01091-z.

Correspondence and requests for materials should be addressed to Patrick Mehlen or Daniel J. Liebl.

Reprints and permission information is available at http://www.nature.com/reprints

Publisher's note Springer Nature remains neutral with regard to jurisdictional claims in published maps and institutional affiliations.

Springer Nature or its licensor (e.g. a society or other partner) holds exclusive rights to this article under a publishing agreement with the author(s) or other rightsholder(s); author self-archiving of the accepted manuscript version of this article is solely governed by the terms of such publishing agreement and applicable law.